The Permittivity and AC Conductivity of the Layered Perovskite $[(CH_3)(C_6H_5)_3P]_2HgI_4$

Ahmed A. A. Youssef

Department of Physics, Faculty of Science, University of Cairo, Giza, Egypt

Reprint requests to Dr. A. A. A. Y.

Z. Naturforsch. **57a,** 263–269 (2002); received January 28, 2002

The dielectric permittivity and ac conductivity of bis-(Methyltriphenyl-phosphonium)$_2$tetraiodomercurate (II), $[(CH_3)(C_6H_5)_3P]_2HgI_4$, has been measured in at 300–400 K and 0.11–20 kHz. The frequency dependent conductivity is interpreted in terms of the jump relaxation model, where translational and reorientational hopping takes place. The conductivity results were fitted to the law

$$\sigma = \sigma_0 + A_1(T)\,\omega^s + A_2(T)\,\omega^r, \quad \text{with} \quad s < 1 \quad \text{and} \quad r < 2\,.$$

The temperature dependence of the conductivity was fitted to two relaxation processes. The activation energies ΔE_1 and ΔE_2 are frequency dependent and lie in the ranges of 0.8 eV and 0.2 eV. ΔE_1 is associated with translational long range hopping while, ΔE_2 is associated with localized and/or reorientational hopping. PACS Nos. 76, 77.

Key words: AC Permittivity; AC Conductivity; Phase Transition;Dielectric measurement.

1. Introduction

During the last years the electric transport in alkylammonium-metal halide compounds with perovskite-like structure has been studied in our laboratory and elsewhere [1–3]. In addition to their technological importance in numerous electrochemical devices, such as fuel cells and chemical sensors [4], these materials provide good models for transport in biological systems [5]. Among these materials are compounds of the type $[(CH_3)_4N]_2MX_4$, and $[(C_2H_5)_4N]_2MX_4$, with M = first raw transition metal ion and X = Cl, Br and/or I.

X-ray diffraction studies showed that the tetramethylammonium salts $[(CH_3)_4N]_2MX_4$, and tetramethylphosphonium salts, $[(CH_3)_4P]_2MX_4$, are isostructural with the P121/c1 phase at room temperature [6, 7]. The room temperature structure of $[(CH_3)_4Z]_2MX_4$ where Z = As and/or P and M = Co^{2+} or Zn^{+2} [8–10], consists of alternating layers of tetrahedral $[(CH_3)_4Z]^+$ and $[MX_4]^{-2}$, i.e. the $[(CH_3)_4Z]^+$ ions are intercalated between the $[MX_4]^{-2}$ ions, the latter being stacked perpendicular to the c-axis. The transition temperatures of three members are listed in Table 1. No permanent dipole moments are present in these structures at room temperature [2]. In analogy to $[(CH_3)_4N]_2MX_4$, the transition of $[(CH_3)_4P]_2MX_4$ probably corresponds to the prototype β-K_2SO_4 Pmcn phases.

Table 1. Transition temperatures of the cited materials.

Material	T_1 (K)	T_2 (K)	Reference
$[(CH_3)(C_6H_5)_3P]_2MnCl_4$		368*	[12]
$[(CH_3)(C_6H_5)_2P]_2CuCl_4$	378**	411*	[11]
$[(CH_3)_4P]_2CuCl_4$	345	381	[10]

* first order, ** second order.

In our laboratory the new family of (methyltriphenylphosphonium)$_2MX_4$, $[(CH_3)(C_6H_5)_3P]_2MX_4$ where M = Mn^{+2}, Co^{+2}, Cu^{+2}, Hg^{+2} and Pb^{+2} and X = Cl was synthesized [11–12]. The electric properties of the Mn^{+2} and Cu^{+2} salts indicated the presence of structural phase transitions at 378 K and 411 K for the Cu^{+2} and at 368 K for the Mn^{+2} salts [11, 12]. The conductivities were found to be frequency dependent. Translational motion of the protons and reorientational hopping between equivalent sites of the metal chloride and the phenyl groups are responsible for the observed conductivity at low temperatures (T < 365 K), while overlap of large polarons predominates at higher temperatures.

In an attempt to learn about the effect of the cation's size and geometry on the phase transition and the electric behavior in this class of compounds, the methyltriphenylphosphonium ion instead of the tetramethyl ion was studied.

The investigations comprised of the thermal behavior (differential thermal analysis), electric permittivity and ac conductivity of $[(CH_3)(C_6H_5)_3P]_2HgI_4$ at 300–400 K and 110 Hz – 20 kHz.

2. Experimental

2.1. Sample Preparation

The material was prepared by mixing equimolar amounts of methyltriphenyl phosphonium iodide and HgI_2 in acidified alcoholic solution. The mixture was kept at 80 °C for two hours and then cooled gradually to room temperature. Cream colored powder fell out. The material was recrystallized from a mixture of alcohol and ether, and then dried under vacuum. The chemical analysis, carried out at the microanalysis unit at the University of Cairo, showed that the compound had the wanted composition. Infra red spectra between 4000 and 200 cm^{-1} were obtained on an FTIR5000 spectrometer, and confirmed the formation of the desired material [11, 12].

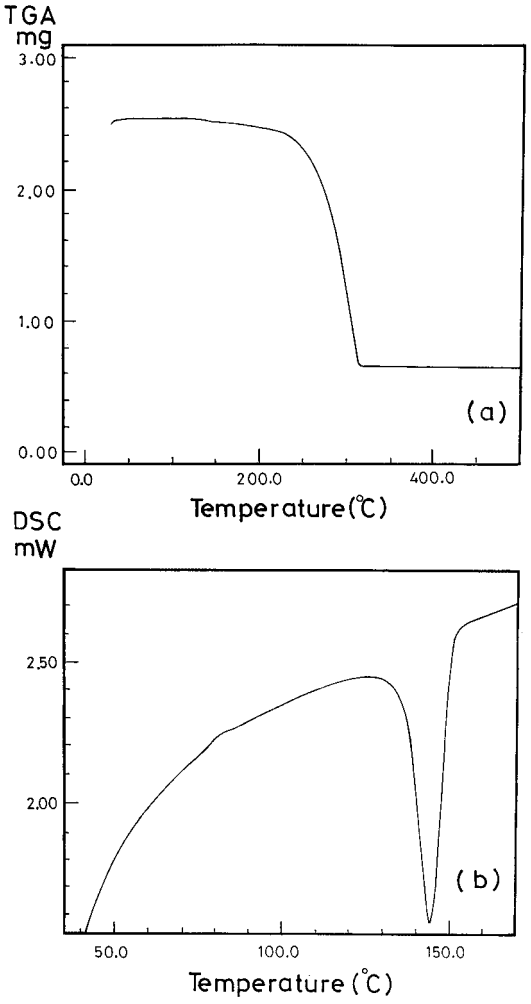

Fig. 1. (a) Thermogravimetric graph (TGA) of $[(CH_3)(C_6H_5)_3P]_2HgI_4$. (b) Differential scanning thermograph (DSC) of $[(CH_3)(C_6H_5)_3P]_2HgI_4$.

2.2. Differential Scanning (DSC) Measurements

Thermogravimetric analysis (TGA) as well as differential thermal scanning (DSC) were performed on a Shimadzu (50) differential scanning analyzer with a scanning speed of 5 °C/min.

2.3. Electric Measurements

The measurements were done with pellets pressed under 2 tons/cm^2, each 8 mm in diameter and 1.0 mm thick. The measuring technique is discussed in [13]. The pellets were coated with silver paste to ensure good electrical contact. The permittivity was measured from 110 Hz to 20 kHz while heating the sample from 300 K to 400 K.

3. Results and Discussion

3.1. Differential Thermal Analysis

The TGA thermograph of $[(CH_3)(C_6H_5)_3P]_2HgI_4$ in the temperature range 300–600 K is shown in Figure 1(a). The graph indicates that the material is stable up to 500 K, at which temperature a loss of weight is noted. The DSC thermograph is shown in Figure 1(b). It reveals a large endothermic peak at $T \approx 420$ k which corresponds to the melting point of the material. No endothermic peaks, indicative of structural phase changes in the temperature range studied, were observed.

3.2. Dielectric Permittivity

Figure 2 shows the real (ε') and imaginary (ε'') parts of the dielectric constant as functions of temperature between 300 and 380 K at frequencies between 110 Hz – 20 kHz. Only seven frequencies are shown for clarity. The real part (ε') is almost temperature independent below 350 K, and it shows a weak frequency dispersion. At higher temperatures a strong temperature dependence and frequency dispersion is noted. The temperature at which the dielectric constant starts to increase rapidly increases for higher frequencies.

3.3. Dielectric Modulus

The dependence of the permittivity on the frequency ω shows an apparent dispersion (Fig. 2). This dispersion

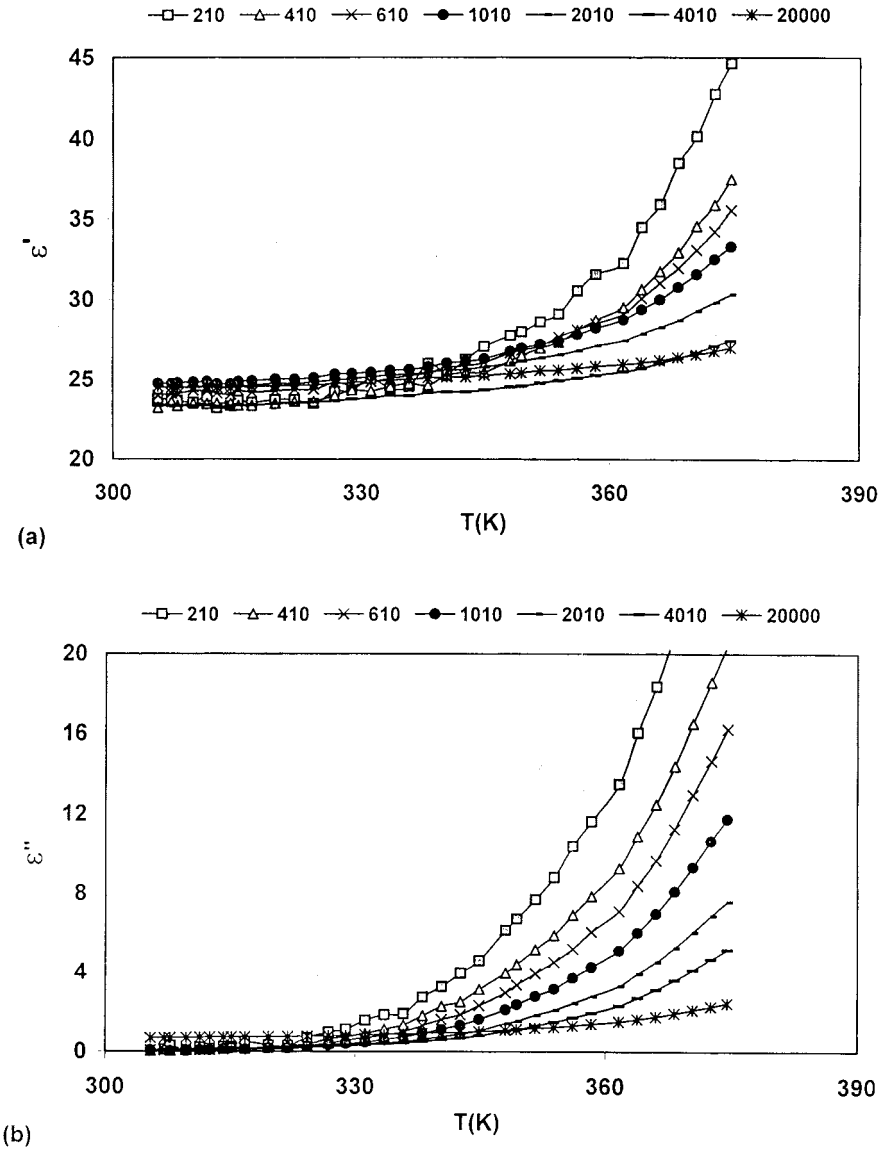

Fig. 2. (a) The real part of the dielectric permittivity (ε') as a function of temperature at selected frequencies. (b) The imaginary part of the dielectric permittivity (ε'') as a function of temperature at selected frequencies (in Hz).

arises from the electrode polarization, which is determined by the sample dimension and/or the nature of the electrode surface. Macedo et al. have introduced the electrical modulus $M^* = 1/\varepsilon^*$ to overcome the effect of electrode polarization [14]. The imaginary part M'' of the complex electric modulus $M^* = M' + iM''$ does not include a contribution from the electrode effect. The frequency and temperature dependence of M' and M'' as function of ln ω are shown in Figs. 3(a) and 3(b), respectively. The plots show features of ionic conduction, namely an *S* shaped dispersion in M' and a peak in M'' [14]. The relaxation peak moves through the temperature "window" or frequency "window" as the temperature and/or frequency changes. It is to be noted that, although the peak shifts its position, its amplitudes is unaffected by the temperature or frequency. The complex modulus plots at 345–375 K are shown in Fig. 3(c). It shows semi circles from which values of $\varepsilon_\infty = 25$ and $\omega\tau = 1$ are obtained. The frequency at $\omega\tau = 1$ is plotted versus the reciprocal temperature in Fig. 3(d). The relaxation behav-

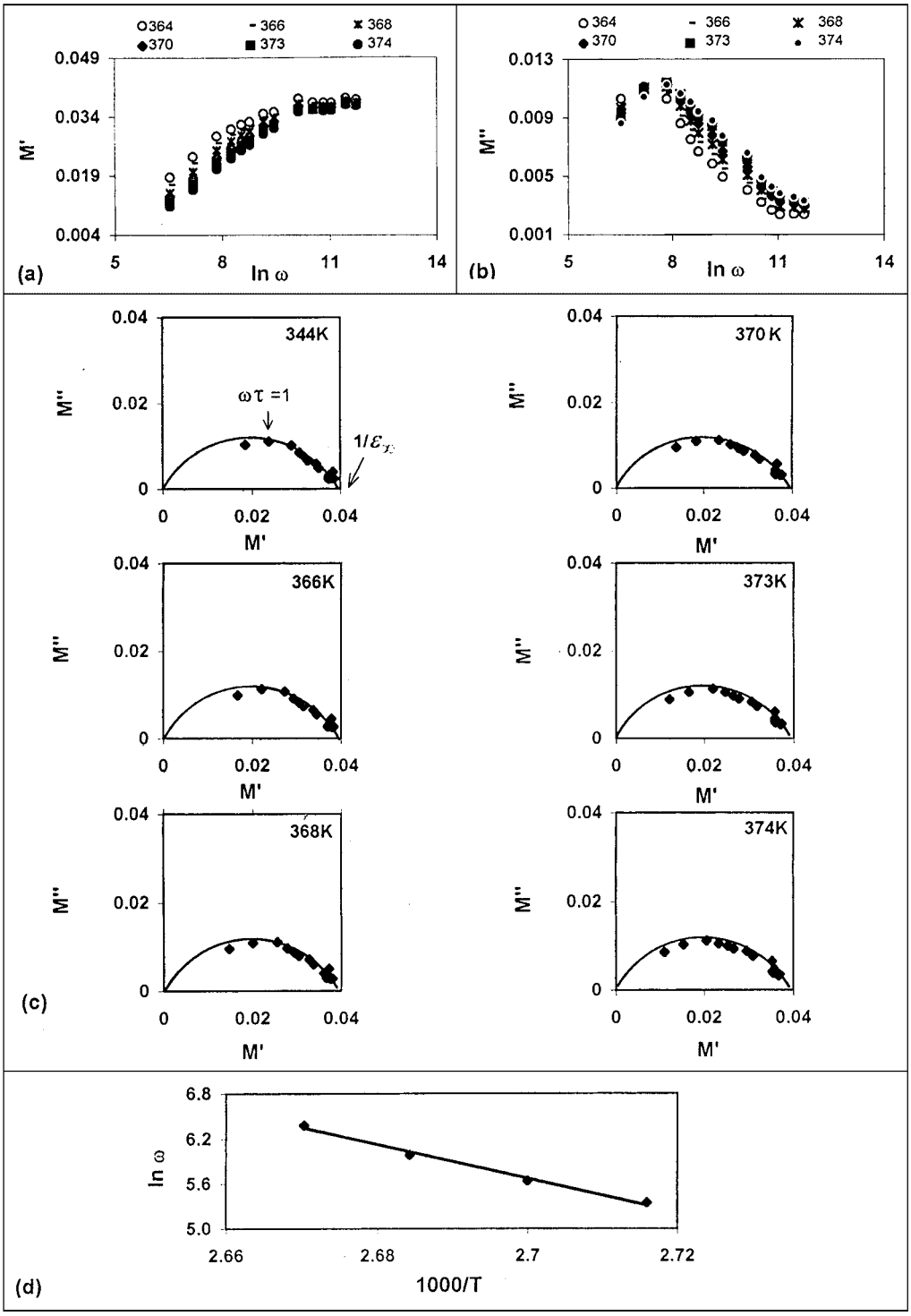

Fig. 3. (a) Frequency dependence of the real (M') part of the complex modulus at selected temperatures (in K). (b) Frequency dependence of the imaginary (M'') part of the complex modulus at selected temperatures (in K). (c) Complex modulus plots M' vs. M''. (d) Frequency of the maximum ($M' - M''$) plots versus reciprocal temperature.

ior can be analyzed assuming the simple exponential activation law

$$f = f_0 \exp(-E_a/T), \quad (1)$$

which yields the activation energy $E_a = 1.92$ eV. It is to be noted that the range of temperature in which (1) applies is limited (345 K < T < 375 K) due to large scattering of data at lower temperatures.

3.4. Conductivity

a) Frequency dependent conductivity

Figure 4(a) shows the variation of the conductivity with frequency at different temperatures. Most previously studied isomorphous perovskite materials in our laboratory [3, 11–13] and elsewhere [15, 16], were found to follow a universal power law

$$\sigma_{ac} = A(T)\,\omega^{s(T)}, \quad (2)$$

where $0 < s < 1$. The relation between σ and ω is usually fall linear in the double-logarithmic presentation, and the slopes of the lines, varying with temperature, are related to the conduction mechanism [16].

It is clear from the Fig. 4(a) that the results do not follow the simple power law relation given by (2). The low frequency ac conductivity (region I) is characterized by a linear response with nearly equal slopes at different temperatures for $T \geq 324$ K. The onset of the characteristic dispersion (region II), at the high frequency end of region I shifts towards higher frequencies with increasing temperature. The slopes of the $\ln\sigma - \ln\omega$-plots in the dispersion region II are strongly temperature dependent. In the jump relaxation model (JRM), introduced by Funke to account for ionic conduction in solids [17], there is a high probability for a jumping ion to jump back (unsuccessful hop). However, if the neighborhood becomes relaxed with respect to the ion's position, the ion stays in the new site. The conductivity in the low frequency region is associated with successful hops. Beyond the low frequency region many hops are unsuccessful, and as the frequency increases, more hops are unsuccessful. The change in the ratio of successful to unsuccessful hops results in the dispersive conductivity. The JRM suggests that different activation energies are associated with unsuccessful and successful hopping processes. Applying the JRM to the frequency response of the conductivity for the present material, it was possible to fit the data to a double power law:

$$\sigma_{ac} = A_1(T)\,\omega^{s(T)} + A_2(T)\,\omega^{r(T)}, \quad (3)$$

where $s < 1$ corresponds to the translational hopping motion and $r < 2$ corresponds to a localized or reorientational hopping motion [17]. Values of s and r obtained from the fitted data are plotted as functions of temperature in Figure 4(b).

b) Temperature dependent conductivity

The extrapolation of the frequency dependent electrical conductivity to $\omega = 0$ yields the dc conductivity. Plots of the obtained $\sigma_{dc}(T)$ as function of $1/T$ gives an activation energy $\Delta E_{dc} = 0.86$ eV. The Arrhenius relation of the conductivity at selected frequencies is seen in Figure 4(c). The plots indicate that the equation

$$\sigma = \sigma_0 + A_1 \exp(-\Delta E_1/kT) \quad (4)$$

is obeyed in the frequency range $f \leq 2$ kHz. It also indicates that there must be different relaxation processes with different activation energies for $f > 2$ kHz. Thus the temperature dependent conductivity for $f > 2$ kHz was fitted to

$$\sigma = A_1 \exp(-\Delta E_1/kT) + A_2 \exp(-\Delta E_2/kT). \quad (5)$$

The least squares fit parameters obtained for different frequencies are given in Table 2. It is to be pointed out that at $f \leq 2$ kHz the data in the lower temperature region (305 < T < 314 K) were not included in the fit as there is a large scattering in this frequency and temperature range.

Table 2. Results of fitting the electrical conductivity at selected frequencies to equations (4) and (5).

f (kHz)	A_1 (Ohm · cm)$^{-1}$	ΔE_1 (eV)	A_2 (Ohm · cm)$^{-1}$	ΔE_2 (eV)	Eq. used
0.4	$1.9 \cdot 10^3$	0.82	–	–	(4)
0.81	$6.0 \cdot 10^3$	0.82	–	–	(4)
4.01	$1.07 \cdot 10^4$	0.74	$1.9 \cdot 10^{-4}$	0.24	(5)
15.0	$2.66 \cdot 10^4$	0.76	$2.16 \cdot 10^{-6}$	0.27	(5)

For $F > 2$ kHz and at low temperatures, the activation energies ΔE_2 calculated using (5) characterize a relaxation process whose onset shifts towards higher temperatures with increasing frequency, where the activation energy ΔE_1 characterizes a second relaxation process and lies in the range of ~ 0.76 – 0.74 eV.

The frequency response of the conductivity is interpreted in terms of the jump relaxation model, where the conduction is due to translational and localized hop-

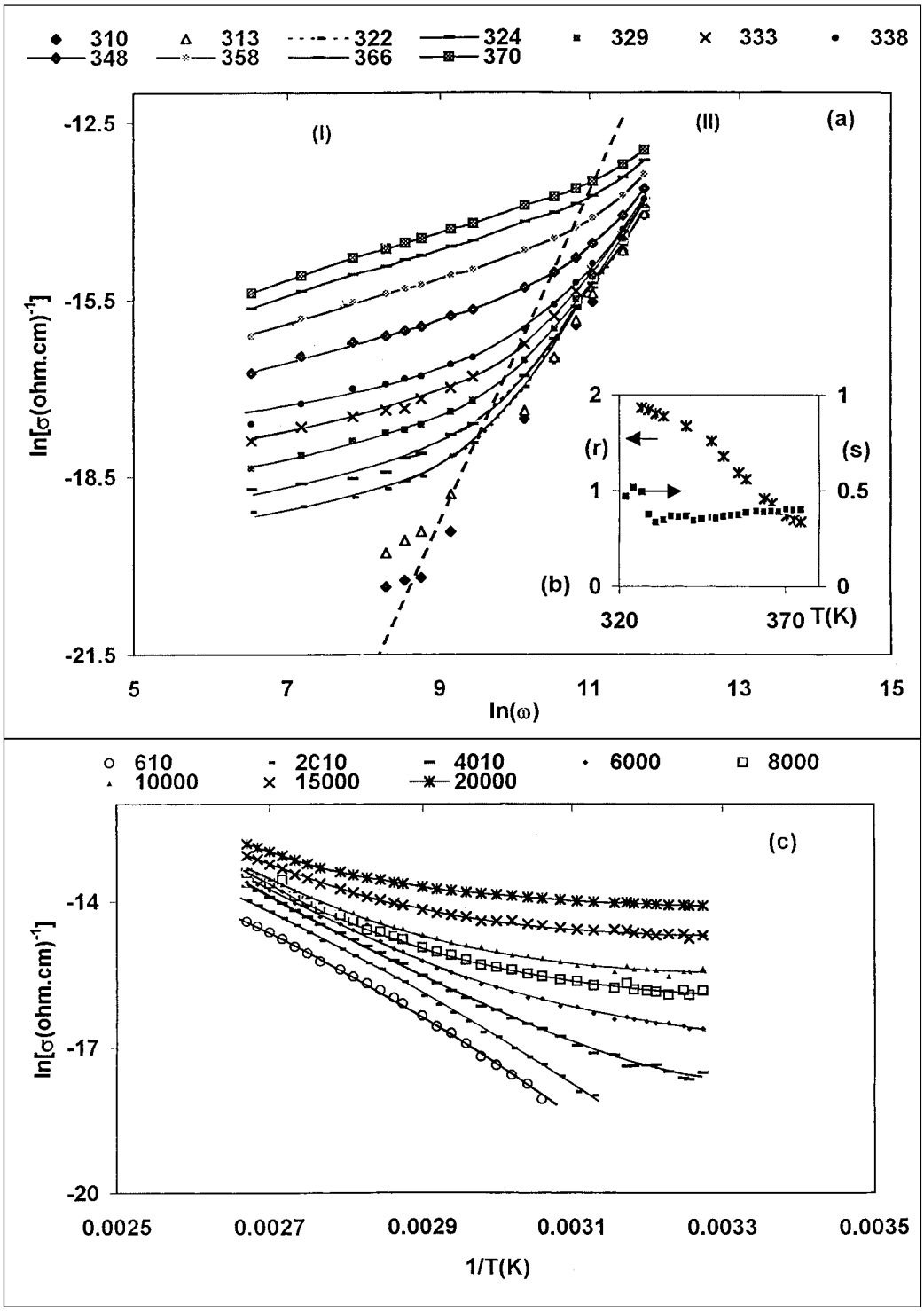

Fig. 4. (a) Frequency dependence of the ac conductivity at different temperatures (in K). Lines represent the fitted results to the data points. (b) Variation of the universal exponents *s* and *r* as a function temperature. (c) Arrhenius plot of the conductivity as a function temperature at selected frequencies (in Hz). Lines represent the fitted results to the data points.

ping. The translational hopping gives the long-range electrical transport in the limit of very long times, i.e. as the frequency approaches zero. The activation energy in the dc conduction process, ($\Delta E_{dc} \sim 0.86$ eV), is of the same order as ΔE_1, as seen in Table 2. Hence ΔE_1 can be associated with successful ionic hopping at low frequencies (region (I)).

The dispersive behavior of the conductivity vs. frequency (region (II)) is associated with the activation energy ΔE_2. In this frequency range the observation time is too short for all jumps to be successful because the neighborhood cannot completely relax to the new position of the ion after its jump. As a result, the activation energy involved in this reorientational hopping is smaller than that involved in the long-range diffusive conduction.

Conclusion

1. The low frequency high temperature region is characterized by a frequency independent activation energy of (0.82 ± 0.04) eV which is very close to that for the dc conduction.

2. The best fit of the conductivity in the dispersive region is obtained using a two-term power law dependence on frequency. The exponent $s < 1$ characterizes the low frequency region, corresponding to translational ion hopping. The exponent $r < 2$ indicates the existence of well localized relaxation process, the activation energy ΔE_2 of which is ascribed to reorientational ionic hopping.

3. In comparing the results of the $[(CH_3)(C_6H_5)_3P]_2HgI_4$ to other members of the series one finds that there are no structural phase transitions for this material at the temperatures investigated, contrary to the case of $[(CH_3)(C_6H_5)_3P]_2MnCl_4$ and $[(CH_3)(C_6H_5)_3P]_2CuCl_4$ [11, 12]. This may indicate the possibility of a dependence of the phase transitions on the type of ion present, its electronegativity, its size as well as the bond strength it forms with the type of halide ion used. It is important to point out that the absence of a structural phase transition in this material in the temperature-range investigated does not rule out a possible structural phase change at lower temperature which is currently being investigated.

4. The conductivity behavior is interpreted in terms of the jump relaxation model, as was done for $[(CH_3)(C_6H_5)_3P]_2MnCl_4$.

[1] M. F. Mostafa and A. A. A. Youssef, Z. Naturforsch. **56a,** 568 (2001).
[2] A. J. Wolthius, W. J. Huiskamp, L. J. DeJongh, and R. L. Carlin, Physica **B 42,** 301 (1986).
[3] M. F. Mostafa, M. El Nimer, and F. Richa, Phys. Scr. **43,** 541 (1991).
[4] V. B. Kapustianik, S. Sveleba, R. Tchukvinskyi, Yu. Korchak, V. Makryi, I. Polovinko, and Z. Trybula, Phys. Stat. Sol. **151**(a), 481 (1995).
[5] B. P. Gaber, P. Yager, and W. L. Petiocolas, Biophys. J. **24,** 677 (1978) and references therein.
[6] M. Presprich and R. D. Willet, Acta Cryst. **C47,** 118 (1991).
[7] M. Kahrizi, S. Misra, J. Kotlinski, M. Steinitz, and T. S. Palmer, Solid State Commun. **79,** 167 (1991).
[8] S. Sawada, Y. Sheroishi, A. Yamamoto, M. Takashige, and M. Matsuo, Phys. Lett. A **67,** 56 (1978).
[9] J. Sugiyama, M. Wada, A. Sawada, and Y. Ishibashi, J. Phys. Soc. Japan **49,** 1405 (1980).
[10] K. Hasebe, H. Mashiyame, and S. Tanisaki, J. Phys. Soc. Japan **49,** 1633 (1980).
[11] M. F. Mostafa, A. S. Atallah, and M. Elessawi, Phase Transitions **64,** 215 (1998).
[12] M. F. Mostafa and A. S. Atallah, Phys. Lett. **A264,** 242 (1999).
[13] M. F. Mostafa, M. M. Abdel-Kadar, A. S. Atallah, and M. El-Nimer, Phys. Stat. Sol. **135(a),** 549 (1993).
[14] P. B. Macedo, C. T. Moynihan, and R. Bose, Phys. Chem. Glass. **13,** 171 (1972).
[15] A. R. Long, Adv. Phys. **31,** 553 (1982).
[16] R. S. Elliot, Adv. Phys. **36,** 135 (1987).
[17] K. Funke, Prog. Solid St. Chem. **22,** 111 (1993).